NASA Technical Paper 3196

May 1992

Effect of Low-Speed Impact Damage and Damage Location on Behavior of Composite Panels

Dawn C. Jegley

NASA

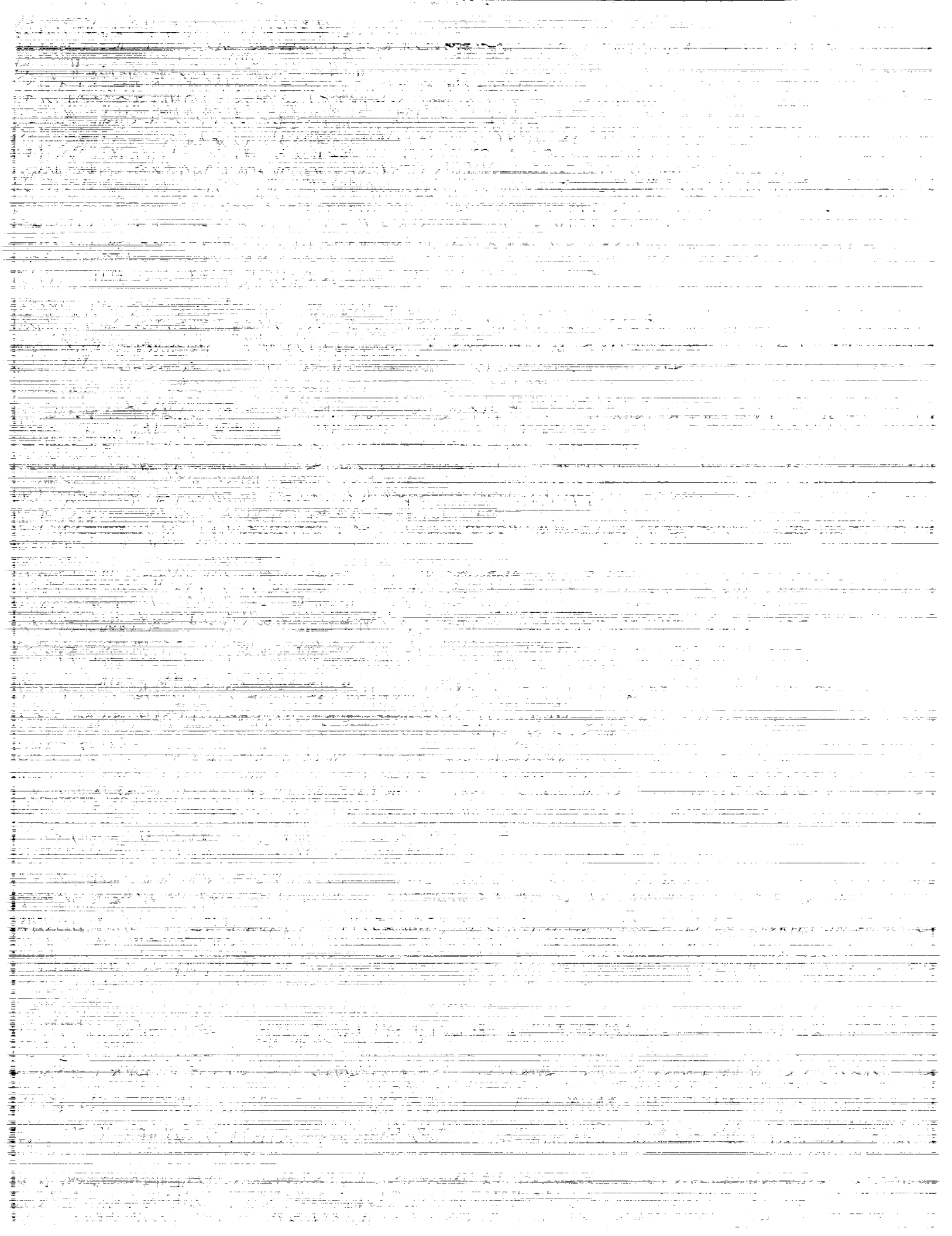

NASA Technical Paper 3196

1992

Effect of Low-Speed Impact Damage and Damage Location on Behavior of Composite Panels

Dawn C. Jegley
Langley Research Center
Hampton, Virginia

NASA
National Aeronautics and Space Administration
Office of Management
Scientific and Technical Information Program

The use of trademarks or names of manufacturers in this report is for accurate reporting and does not constitute an official endorsement, either expressed or implied, of such products or manufacturers by the National Aeronautics and Space Administration.

Symbols

A	initial cross-sectional area of specimen, in^2
b	width of specimen, in.
$D_{11}, D_{22}, D_{16}, D_{26}$	bending stiffnesses, in-lb
L	length of specimen, in.
P	applied load, lb
P_{cr}	buckling load, lb
P_f	failure load, lb
t	thickness of specimen, in.
w	out-of-plane displacement, in.
x	distance from lateral unloaded edge of specimen, in.
y	distance from loaded edge of specimen, in.
δ	end-shortening, in.

Summary

The effect of low-speed impact damage on the compression and tension strength of thin (less than 0.05 in. thick) and moderately thick (between 0.12 and 0.17 in. thick) composite specimens was investigated. Impact speeds ranged from 50 to 550 ft/sec with corresponding impact energies from 0.25 to 30.7 ft-lb. Impact locations were at the center of the specimen or near a lateral unloaded edge. In this study, thin tension-loaded or compression-loaded specimens with only 90° and ±45° plies that were impacted away from the unloaded edge suffered less reduction in maximum load-carrying capability because of impact damage than the same specimens impacted near the unloaded edge.

Unlike the thin laminates, failure loads of thicker compression-loaded specimens with a similar stacking sequence were independent of impact location. Failure loads of thin tension-loaded specimens with 0° plies were also independent of impact location, whereas failure loads of thicker compression-loaded specimens with 0° plies were dependent upon impact location. A finite-element analysis of strain distributions across the panel width indicated that high axial strains occurred near the unloaded edges of post-buckled panels. Thus, impacts near the unloaded edge would significantly affect the behavior of post-buckled panels.

Introduction

For composite parts to be used on primary structures of aircraft, the effect of low-speed impact damage on the behavior of these structures must be understood. Impact damage followed by compression or tension loading is an important condition to be considered in the design of aircraft with composite structures. Both thicker laminates for wing panels and thinner laminates for fuselage skins must be studied.

Much work has been done on the effect of impact damage in the center of a relatively thick specimen loaded in compression (e.g., refs. 1 through 3). This type of impact damage is representative of impact damage in a wing panel away from a supported edge or a stiffener. Less work has been done on impact damage near a support location or a stiffener on thinner specimens. However, impact damage near a stiffener or a supported edge can be a critical problem in compression-loaded structures. (See ref. 4.) Moreover, damage tolerance criteria for thick specimens, such as allowable indentation depth, are not always applicable to thin specimens.

The effect of impact location on tension-loaded panels is also largely unexplored, although fuselage structures carry tensile as well as compressive loads. Some data on tension-loaded specimens impacted away from a support location are presented in references 5 and 6, but more work needs to be done to quantify the effects of panel thickness and impact location on structural performance.

The objectives of this paper are to discuss the effect of varying the location of impact damage on failure of thin and moderately thick composite structures and to provide an explanation for their behavior. Presented are the results of an investigation of the behavior of graphite-epoxy and graphite-thermoplastic specimens subjected to low-speed impact damage at the center of the specimen and near an unloaded edge. Tension-loaded specimens, whose behavior is dependent upon material characteristics, are discussed first. Compression-loaded specimens, whose behavior is dependent upon both material characteristics and structural parameters, are discussed last.

Test Specimens

The graphite-epoxy specimens tested in this investigation were fabricated from commercially available Hercules AS4 graphite fiber and 3502 thermosetting epoxy resin. The graphite-thermoplastic specimens were fabricated from Hercules AS4 graphite fiber and ICI PEEK thermoplastic resin. All graphite-epoxy and some graphite-thermoplastic specimens were fabricated from unidirectional tape. The remaining graphite-thermoplastic specimens were fabricated from woven fabric, in which the +45° and −45° fibers were woven together. The specimens tested in this study were made from the four stacking sequences $[(\pm 45)_2/\overline{90}]_s$, $[(\pm 45)_2/90]_{3s}$, $[\pm 45/0_2]_s$, and $[\pm 45/0_2]_{3s}$, which include a range of thicknesses. Specimen dimensions are shown in table I. All specimens were nominally 10 or 14 in. long and either 3, 4, or 10 in. wide with width-to-thickness ratios from 18 to 240. All specimens were ultrasonically C-scanned to establish specimen quality prior to testing. Tabs were bonded to the tension-loaded specimens to prevent the grips of the testing machine from inducing damage. The configuration of a typical tension specimen is shown in figure 1(a). The loaded ends of each compression specimen were machined flat and parallel in order to permit uniform end displacement.

Apparatus and Tests

Tension Tests

Test specimens were slowly loaded in tension in a hydraulic test machine with hydraulic grips. The

unloaded edges were unsupported during the test. The applied load and change in specimen length were recorded at regular intervals during the test.

Compression Tests

Test specimens were slowly loaded in uniaxial compression by using a hydraulic testing machine. The loaded ends of the specimen were clamped by fixtures during testing, and the unloaded lateral edges were simply supported by knife-edge restraints to prevent the specimen from buckling as a wide column. A typical compression specimen mounted in the support fixture is shown in figure 1(b). Electrical resistance strain gauges were used to monitor strains, and direct current differential transformers were used to monitor displacements. Figure 1(b) also shows typical locations of back-to-back strain gauges that were used to monitor far-field laminate strains. All specimens loaded in compression were painted white on one side to provide a reflective surface so that a moiré fringe technique could be used to monitor out-of-plane deformation patterns. The applied load, the displacement of the loading platen, and the strain-gauge signals were recorded at regular intervals during the test.

Impact Damage

A procedure described in reference 7 was used in the current study for impacting specimens. Aluminum spheres 0.5 in. in diameter were used as impact projectiles that were directed normal to the plane of the specimen at speeds from 50 to 550 ft/sec. One specimen of each type was not impacted and used as a reference or control, whereas the remaining specimens were impacted prior to loading. All impacted specimens were impacted at the axial center and either at the lateral center or near a lateral unloaded edge. Compression-loaded specimens were placed in the test fixture prior to impact. Lateral locations of impact sites are indicated in figure 1. Since impact speed alone does not fully describe an impact event, the range of impact speeds considered and the corresponding impact energy is shown in table II.

Analytical Model

Finite-element models were developed for the graphite-epoxy control specimens that were compression loaded. A uniform grid of quadrilateral plate elements was used. The number of elements used to model each specimen depended upon the specimen dimensions, but in each case the elements used were approximately square. At least 30 elements were used in the axial direction for each model. To simulate clamped conditions, no displacements or rotations were permitted on one end of the specimen and only the axial displacement was permitted on the opposite (loaded) end. The axial displacement was forced to be constant along the loaded edge. To simulate the simply supported edges, no out-of-plane displacements along the unloaded lateral edges were permitted. All analytical results are based on material properties given in table III and a nonlinear analysis using the finite-element computer code STAGS (ref. 8).

Results and Discussion

Test results for specimens constructed with the four stacking sequences given in table I are presented in this section. A comparison is made between specimens with the same stacking sequence that were impacted with the same impact energy in the center of the test section and those impacted near a lateral unloaded edge. The unloaded edges were free for tension specimens, and simply supported for compression specimens. Experimentally determined failure loads and strains are discussed for tension-loaded specimens; then, experimentally determined failure loads, buckling loads, strain distributions, and out-of-plane deformations are discussed for compression-loaded specimens.

Finite-element predictions of displacements and strains and experimental results are presented for specimens loaded into the postbuckling range. Results are presented in terms of *normalized load* (i.e., load divided by the cross-sectional area of the specimen) and *normalized end-shortening* (i.e., end-shortening divided by the length of the specimen), not as average stress and average strain. The terms "average stress" and "average strain" could be misleading, since stresses and strains in the specimen after buckling are not constant across the width of the panel.

Tension-Loaded Specimens

Graphite-epoxy specimens constructed with two different stacking sequences were loaded in tension. One control specimen (i.e., without impact damage) of each stacking sequence was tested. All impacted specimens were impacted at the axial center. One half the impacted specimens were impacted at the axial and lateral center ($x/b = 0.5$, where x is the distance from the lateral unloaded edge of the specimen to the impact site and b is the width of the specimen) and one half were impacted 0.75 in. from a lateral unloaded edge ($x/b = 0.25$). All specimens

were loaded to failure and showed extensive damage because of failure. Control specimens failed near the tabs, whereas impact-damaged specimens failed through the impact site. The normalized failure load (i.e., failure load P_f divided by initial cross-sectional area A) of the control specimens is shown in table I. The nominal impact speeds, impact locations, and normalized failure loads are shown in table IV for all impacted, tension-loaded specimens.

The effect of impact damage on the maximum load-carrying capability of the tension-loaded specimens is presented in figure 2, which shows the relationship between normalized failure load and impact speed. The circular symbols in the figure represent failures of specimens impacted near an unloaded edge, and the square symbols represent failure of specimens impacted in the center of the specimen. Impacts that caused no visible damage are represented by open symbols. Impacts that caused visible damage are represented by shaded symbols if the impactor did not pass through the specimen and by solid symbols if the impactor did pass through the specimen.

The maximum reduction in load-carrying capability demonstrated in the center-impacted specimens was 32 and 25 percent of the load-carrying capability of the corresponding undamaged (control) specimens for the $[(\pm 45)_2/\overline{90}]_s$ and $[\pm 45/0_2]_s$ specimens, respectively. In each case, the maximum reduction for the center-impacted specimens occurred for impact speeds of 300 ft/sec. The maximum reduction for side-impacted specimens was 49 and 30 percent of the load-carrying capability of the control specimens for the $[(\pm 45)_2/\overline{90}]_s$ and $[\pm 45/0_2]_s$ specimens, respectively.

For the $[(\pm 45)_2/\overline{90}]_s$ specimens, the center-impacted specimens carried slightly more load at failure than the side-impacted specimens for all impact speeds considered. However, the side-impacted $[\pm 45/0_2]_s$ specimen impacted at 400 ft/sec had a higher failure load than the center-impacted specimen impacted at the same speed. This result suggests that impact location had no influence on maximum load-carrying capability for $[\pm 45/0_2]_s$ specimens when loaded in tension. The 400 ft/sec impacts caused less reduction in load-carrying capability than the 300 ft/sec impacts for the $[\pm 45/0_2]_s$ specimens. Reference 6 describes the same behavior for $[0/90]_{3s}$ specimens.

In the study described in reference 6, the most damage occurred when the impact speed was just sufficient for the impactor to pass through the specimen. Different types of damage are caused by impacts at different speeds. For example, low-speed impacts cause delaminations within the specimen. Higher speed impacts, in which the impactor does not pass through the specimen, and impacts in which the impactor barely passes through the specimen, cause delaminations and severe damage to the back of the specimen, including fiber breakage. Very high speed impacts, in which the impactor passes through the specimen, cause very high stress at the impact site and less cracking away from the impact site. These different types of damage can lead to different failure modes and different amounts of reduction in maximum load-carrying capability.

Compression-Loaded Specimens

Control Specimens

Control specimens for each stacking sequence were loaded in compression. Six control specimens with stacking sequence $[(\pm 45)_2/\overline{90}]_s$ were loaded to failure. A 3-in-wide specimen and a 4-in-wide specimen were each constructed from graphite-epoxy tape, graphite-thermoplastic tape, and graphite-thermoplastic fabric. The 3-in-wide specimens buckled into one transverse and four axial half-waves of nearly equal wavelength, then failed at specimen midlength (along a nodal line). The 4-in-wide specimens buckled into one transverse and three axial half-waves, then failed at a nodal line. Each specimen carried load well into the postbuckling range. Normalized failure loads are shown in table I.

Two moderately thick control specimens with stacking sequence $[(\pm 45)_2/90]_{3s}$ were constructed from graphite-epoxy tape and loaded to failure. One specimen was 3 in. wide and one was 4 in. wide. Both specimens buckled into one transverse and three axial half-waves immediately prior to failure. The 3-in-wide specimen failed through the center of the specimen (not along a nodal line). The 4-in-wide specimen, however, failed at a nodal line. Normalized failure loads are shown in table I.

One thin control specimen with stacking sequence $[\pm 45/0_2]_s$ and one moderately thick control specimen with stacking sequence $[\pm 45/0_2]_{3s}$ were made from graphite-epoxy tape and tested. Each specimen was 10 in. wide and 14 in. long. These control specimens buckled into one half-wave in each direction prior to failure near a loaded edge. The normalized failure load of the $[\pm 45/0_2]_{3s}$ control specimen is shown in table I. The $[\pm 45/0_2]_s$ control specimen was not loaded to failure.

Impact-Damaged Specimens

All remaining compression-loaded specimens were subjected to impact damage prior to loading. Nominal impact speeds, impact locations, and normalized failure loads are shown in tables V, VI, and VII for the compression-loaded specimens with 3-, 4-, and 10-in. widths, respectively.

$[(\pm 45)_2/\overline{90}]_S$ *specimens.* The relationship between impact speed and normalized failure load is shown in figures 3(a), (b), and (c) for specimens fabricated from graphite-epoxy tape, graphite-thermoplastic tape, and graphite-thermoplastic fabric, respectively. The circular symbols in each figure represent the failure of the side-impacted specimens and the square symbols represent the failure of center-impacted specimens. Impacts that caused no visible damage are represented by open symbols. Impacts that caused visible damage are represented by shaded symbols if the impactor did not pass through the specimen and by solid symbols if it did.

Specimens subjected to impact speeds of less than about 200 ft/sec buckled into four axial half-waves and then failed at the nodal line through the impact site. Specimens subjected to higher impact speeds buckled into three, four, or five axial half-waves along the length and failed through the impact site whether the impact site was located on a nodal line. Each specimen failed by transverse cracking and many also exhibited off-axis cracking and fiber separation on the side opposite the impact site.

Impacts at 100 ft/sec caused no reduction in maximum load-carrying capability. However, the results show the normalized failure load was significantly reduced for each type of specimen as impact speed increased from 100 to 300 ft/sec. For the graphite-epoxy specimens, a center impact can reduce the maximum load-carrying capability of a specimen by up to 12 percent compared with that of an undamaged specimen. However, for the graphite-thermoplastic specimens, a center impact can reduce the maximum load-carrying capability by 30–35 percent. The impact speed causing the most reduction in maximum load-carrying capability was 225 ft/sec for the graphite-epoxy specimen and 300 ft/sec for the graphite-thermoplastic specimen.

The results shown in figure 3 indicate that the normalized failure load depends on impact location. An impact 0.75 in. from the lateral unloaded edge of a 3-in-wide specimen caused a reduction in maximum load-carrying capability of about 35 percent for each type of specimen (i.e., three times the reduction in the graphite-epoxy center-impacted specimens, but about the same as the reduction in the graphite-thermoplastic center-impacted specimens). The effect of impact location on maximum load-carrying capability was more significant for graphite-epoxy specimens than for graphite-thermoplastic specimens. However, the trend was the same for both materials. A side impact reduced the maximum load-carrying capability of the specimens by at least as much as a central impact for a given impact speed.

Nonvisible damage did not reduce the maximum load-carrying capability of the three types of specimens shown in figure 3, and the impact speed that produced barely visible damage was approximately 170 ft/sec. Impacts causing visible damage also caused an extensive reduction in maximum load-carrying capability. In general, the most severe reduction occurred when the impact speed was approximately the speed necessary to cause the impactor to pass through the specimen. This speed was approximately 240, 325, and 275 ft/sec for the graphite-epoxy tape, the graphite-thermoplastic tape, and the graphite-thermoplastic fabric specimens, respectively.

An impactor that passed through the specimen at high speed (e.g., 500 ft/sec) caused less damage than an impactor that bounced off the specimen. This difference in the amount of damage explains why a damaged specimen has a higher maximum load-carrying capability with a through penetration than without. Ultrasonic C-scans of specimens after impact and before compressive loading indicate that the damage area for the graphite-thermoplastic specimens was significantly less for very high speed impacts compared with impacts in which the impactor barely passes through the specimen. A small decrease in damage area was seen for very high speed impacts for the graphite-epoxy specimens. However, the failure load does not always correlate with damage area determined by C-scan, as reference 3 shows for several stacking sequences. This lack of correlation is attributed to the fact that the C-scan indicates a total damage area in a qualitative manner, not a specific amount and type of damage (i.e., number and location of delaminations) in the area.

The relationship between normalized failure load and impact location is shown in figure 4 for 4-in-wide specimens impacted at several locations across their widths at a speed of approximately 450 ft/sec. (At this speed, the impactor passed through the specimens.) For each specimen, the center impacts caused little reduction in maximum load-carrying capability, but the side impacts caused a significant reduction. The closer the impacts were to the edge of

the specimen, the more the maximum load-carrying capability was reduced. An explanation for why a side impact causes more reduction in maximum load-carrying capability than a center impact is presented at the end of this section.

The experimentally determined normalized load versus normalized end-shortening of four impacted graphite-epoxy specimens is shown in figure 5. The load is normalized by the specimen cross-sectional area and the end-shortening is normalized by the specimen length. Two specimens were impacted at 175 ft/sec, in which case damage was barely visible, and two specimens were impacted at 250 ft/sec, in which case the impactor passed through the specimen. Each specimen buckled at a normalized load of approximately 10 ksi and the prebuckling responses of the side- and center-impacted specimens were the same for both. The primary difference in the postbuckling responses was that the side-impacted specimens failed at much lower loads than the center-impacted specimens.

The displacements and strains in the 4-in-wide control specimen are shown in figure 6. The experimentally determined normalized load versus normalized end-shortening relationship for three 4-in-wide specimens and the analytically determined normalized load versus normalized end-shortening relationship for a 4-in-wide control specimen are shown in figure 6(a). The analytical and experimental results for the control specimen agreed quite well. The control specimen failed at a load 2.61 times the buckling load. Little difference was seen between the results for the center-impacted specimen and the control specimen, but the side-impacted specimen failed at a much lower load, although the overall specimen stiffness seemed to be unaffected by the impact damage.

Figure 6(b) shows the analytically determined out-of-plane displacements w normalized by the specimen thickness t for a specimen loaded in the postbuckling range. The displacements are along the specimen length at the center, at one quarter of the width, and near an unloaded edge. The buckling load of the specimen is represented by P_{cr} and the specimen buckled into one transverse and three axial half-waves. Displacements for 1.22 and 2.55 times the buckling load are shown. The maximum out-of-plane displacement is at the center of the specimen. The highest gradient in out-of-plane deformation is at the nodal lines, at approximately $y/L = 0.33$ and 0.66 where y is the distance from the loaded edge.

The experimentally determined axial membrane strain (i.e., the average of back-to-back strain gauges) across the specimen at a nodal line is shown in figure 6(c) for several values of load P, normalized by the buckling load P_{cr}, in the prebuckling and postbuckling range. In the postbuckling range, the higher the value of P/P_{cr}, the higher the membrane strain is near the unloaded edge of the specimen and the lower the membrane strain is near the center of the specimen. The axial strain distribution across the specimen width at a nodal line just before failure is shown in figure 6(d). The dashed and solid curves represent membrane strains determined analytically and experimentally, respectively (a least-squares fit to the data points was used). The open and solid symbols represent surface strains determined analytically and experimentally, respectively. Slight differences in results at the unloaded edges can be attributed to anisotropic effects since the ratios of the anisotropic terms to the bending stiffnesses are relatively large (i.e., $D_{16}/D_{11} = 0.22$, and $D_{26}/D_{22} = 0.31$). Front and back surface strains differed significantly in the postbuckled specimen, and much higher strains occurred at the edges of the specimen than at the center.

The strain and displacement distributions presented in figure 6 indicate why side impacts have more effect on failure loads than center impacts for these buckled specimens. Prior to buckling, the axial strain is relatively constant across the width of the panel; therefore, impact location has little effect on specimen behavior. At buckling, the loads in the panel redistribute and more load is carried near the supported unloaded edges. The high deformation gradients at the nodal lines and the higher strains near the specimen edges induce transverse shearing loads that cause failure at the nodal lines in undamaged specimens. Impact damage in a region of high strain near an unloaded edge has more effect on strength than impact damage in a region of low strain at the specimen center.

$[(\pm 45)_2/90]_{3s}$ *specimens.* A series of moderately thick 3-in-wide specimens was impacted either in the center of the specimen or 0.7 in. away from an unloaded edge. The relationship between normalized failure load and impact speed is shown in figure 7 for these specimens. The specimen that was impacted in the center at 100 ft/sec buckled into three axial half-waves immediately prior to failure. No other impacted specimen buckled. The most severe reduction in maximum load-carrying capability because of impact damage occurred at a speed of 400 ft/sec, but there appeared to be no difference between the effect of side impact and center impact. The impactor passed through the specimen at speeds greater than about 425 ft/sec and the failure load increased

slightly for speeds of 525 ft/sec because a more ballistic type of damage is induced at very high speeds (ref. 6). Nonvisible damage did not cause a reduction in maximum load-carrying capability, but barely visible damage (impact speeds of 150 ft/sec) caused more than a 40-percent reduction in maximum load-carrying capability compared with the control specimen.

The relationship between normalized failure load and impact location for four 4-in-wide specimens impacted at a speed of 500 ft/sec is shown in figure 8. Impact location appeared to have little effect on failure load. The normalized load versus normalized end-shortening for three specimens impacted at 540 ft/sec is shown in figure 9. The control specimen buckled just before failure, whereas the impacted specimens failed well before buckling occurred. The fact that these impacted specimens did not buckle means that the strain distribution across the specimen width was almost constant at failure.

The measured surface strains, membrane surface strains based on an average of the surface strains, and analytical membrane strains are shown in figure 10 for the control specimen just prior to failure. Surface strains are represented by data points and membrane strains are represented by curves. The results show that no significant difference existed in strain across the specimen width; thus, impact location did not affect maximum load-carrying ability.

$[\pm 45/0_2]_s$ *specimens.* Two 10-in-wide specimens were impacted at a speed of 150 ft/sec and loaded to failure. Impact locations were at the axial center and either at the lateral center or 1 in. from the specimen unloaded edge. Each specimen buckled into one transverse and two axial half-waves then continued to carry load well into the postbuckling range. The specimens then exhibited a mode shape change to three axial half-waves and failed at a loaded edge. The relationship of normalized load versus normalized end-shortening for these two specimens is shown in figure 11. The impact had little effect on the specimen prebuckling behavior, buckling load, or postbuckling behavior.

$[\pm 45/0_2]_{3s}$ *specimens.* Nine specimens were constructed from graphite-epoxy tape and loaded to failure. Each specimen was 14 in. long and 10 in. wide. Each specimen buckled into one half-wave in each direction prior to failure. Failures occurred at a loaded edge in all cases and caused damage growth at the impact sites for the specimens impacted at high-impact speeds. Visible damage was caused by impacts of 300 ft/sec and the impactor passed through the specimen for impacts with speeds greater than 400 ft/sec. Three specimens were impacted at the center, two were impacted 2 in. from an unloaded edge, and two were impacted 1 inch from an unloaded edge; this provided results for impact sites at $x/b = 0.5$, 0.2, and 0.1, respectively.

The relationship between normalized failure load and impact speed is shown in figure 12. Center impacts and impacts at $x/b = 0.2$ did not cause a reduction in maximum load-carrying capability at impact speeds of up to 450 ft/sec. However, impacts at speeds above 300 ft/sec at $x/b = 0.1$ significantly reduced the maximum load-carrying capability. An impact at 450 ft/sec at $x/b = 0.1$ can cause a 30-percent reduction in failure load compared with the control specimen.

The experimentally and analytically determined normalized load versus normalized end-shortening relationships for the control specimen are shown in figure 13. The analytical and experimental results for the control specimen agreed quite well and each method predicted a normalized buckling load of about 6.5 ksi. The specimen failed at 3.1 times the buckling load. The normalized load versus normalized end-shortening behavior of the center-impacted specimen and both of the side-impacted specimens that were impacted at 450 ft/sec are shown in figure 14. Once again, prebuckling behavior was approximately the same for the three specimens, as was their initial postbuckling behavior.

The axial strain distribution across the width of a control specimen at midlength is shown in figure 15. The change in analytically determined strain distribution as the load was increased past the buckling load to specimen failure is shown in figure 15(a), and the experimental and analytical membrane strains at failure are shown in figure 15(b). The data points represent surface strains measured by strain gauges. The solid and dashed curves represent membrane strains determined from averaging back-to-back surface strain-gauge results and from finite-element analysis, respectively. Higher strains occurred at the specimen edges than in the center, as seen before. However, the section of the specimen that experienced higher strains was smaller than that in the previous case.

In $[\pm 45/0_2]_{3s}$ specimens, an impact at width position $x/b = 0.2$ was not as far into the region of high strain as an impact at width position $x/b = 0.25$ in the $[(\pm 45)_2/90]_s$ specimens; thus, the impact at

$x/b = 0.2$ in the $[\pm 45/0_2]_{3s}$ specimens caused less reduction in maximum load-carrying capability than the impacts at $x/b = 0.25$ in the $[\pm 45/0_2]_{3s}$ case. However, an impact at $x/b = 0.1$ in the $[\pm 45/0_2]_{3s}$ specimens was in the region of high axial strain; thus, this impact did significantly affect the maximum load-carrying capability of the specimen. Impact damage location had more effect on maximum load-carrying capability for specimens without 0° plies than for specimens with 0° plies, since stacking sequence influenced how the load was redistributed after buckling.

Concluding Remarks

The behavior of laminated thin and moderately thick graphite-epoxy and graphite-thermoplastic specimens subjected to impact damage and loaded in compression and tension was investigated. Specimens were impacted with a 0.5-in-diameter aluminum sphere at impact speeds of up to 550 ft/sec (impact energy 30.7 ft-lb) either in the center of the specimen or near an unloaded edge prior to loading.

The results of this investigation indicate that impact location in thin tension-loaded specimens dominated by angle plies influences failure load. In these specimens, impacts near an unsupported edge reduced specimen maximum load-carrying capability more than central impacts, which were away from an unsupported edge. However, the failure load of thin tension-loaded specimens with 50 percent 0° plies was independent of impact location. Experimental results and finite-element analysis results of compression-loaded specimens indicate that high axial strains occurred near the simply supported unloaded edges of a postbuckled specimen. These strains led to lower failure loads in specimens impacted near the unloaded edge than in specimens impacted away from an edge. The failure load for damaged specimens that failed prior to buckling was unaffected by the widthwise location of the impact damage. Impact damage to specimens with 0° plies was less dependent upon impact location than impact damage to specimens without 0° plies.

NASA Langley Research Center
Hampton, VA 23665-5225
March 11, 1992

References

1. Starnes, James H., Jr.; and Williams, Jerry G.: Failure Characteristics of Graphite-Epoxy Structural Components Loaded in Compression. *Mechanics of Composite Materials—Recent Advances,* Zvi Hashin and Carl T. Herakovich, eds., Pergamon Press Inc., c.1983, pp. 283–306.

2. Jegley, Dawn C.: *Compression Behavior of Graphite-Thermoplastic and Graphite-Epoxy Panels With Circular Holes or Impact Damage.* NASA TP-3071, 1991.

3. Guynn, E. G.; and O'Brien, T. K.: The Influence of Lay-up and Thickness on Composite Impact Damage and Compression Strength. AIAA-85-0646, Apr. 1985.

4. Starnes, James H., Jr.; and Rouse, Marshall: Postbuckling and Failure Characteristics of Selected Flat Rectangular Graphite-Epoxy Plates Loaded in Compression. *A Collection of Technical Papers AIAA/ASME/ASCE/AHS 22nd Structures, Structural Dynamics & Materials Conference,* Part 1, Apr. 1981, pp. 423–434. (Available as AIAA-81-0543.)

5. Avva, V. Sarma: *Fatigue/Impact Studies in Laminated Composites.* AFWAL-TR-83-3060, U.S. Air Force, May 1983. (Available from DTIC as AD A142 841.)

6. Dorey, Graham: Damage Tolerance and Damage Assessment in Advanced Composites. *Advanced Composites,* Ivana K. Partridge, ed., Elsevier Science Publ. Co., Inc., c.1989, pp. 369–398.

7. Starnes, J. H., Jr.; Rhodes, M. D.; and Williams, J. G.: Effect of Impact Damage and Holes on the Compressive Strength of a Graphite/Epoxy Laminate, *Nondestructive Evaluation and Flaw Criticality for Composite Materials,* R. B. Pipes, ed., ASTM Spec Tech. Publ. 696, c.1979, pp. 145–171.

8. Almroth, B. O.; and Brogan, F. A.: *The STAGS Computer Code.* NASA CR-2950, 1978.

Table I. Stacking Sequence, Average Specimen Dimensions, and Normalized Failure Load of Control Specimen

Stacking sequence	Material (a)	Average thickness, t, in.	Average width, b, in.	Average length, L, in.	Number of specimens tested	Normalized failure load, P_f/A, ksi
Tension-loaded specimens						
$[(\pm 45)_2/\overline{90}]_s$	ge, tape	0.0498	3.00	10.01	7	32.8
$[\pm 45/0_2]_s$	ge, tape	.0435	3.00	10.00	8	128
Compression-loaded specimens						
$[(\pm 45)_2/\overline{90}]_s$	ge, tape	0.0481	3.00	10.00	12	19.7
$[(\pm 45)_2/\overline{90}]_s$	ge, tape	.0479	4.00	10.00	4	15.6
$[(\pm 45)_2/\overline{90}]_s$	gt, tape	.0491	2.99	9.92	14	20.6
$[(\pm 45)_2/\overline{90}]_s$	gt, tape	.0495	4.00	10.00	3	16.4
$[(\pm 45)_2/\overline{90}]_s$	gt, fabric	.0470	3.00	10.00	12	21.2
$[(\pm 45)_2/\overline{90}]_s$	gt, fabric	.0461	4.00	10.00	4	17.8
$[(\pm 45)_2/90]_{3s}$	ge, tape	.1626	3.00	10.00	12	53.0
$[(\pm 45)_2/90]_{3s}$	ge, tape	.1610	4.00	10.00	4	49.4
$[\pm 45/0_2]_s$	ge, tape	.0428	10.00	14.00	3	
$[(\pm 45/0_2]_{3s}$	ge, tape	.1280	10.00	14.00	9	20.4

[a]ge: graphite-epoxy; gt: graphite-thermoplastic; tape: unidirectional tape; fabric: woven fabric with ±45 fibers.

Table II. Relationship Between Impact Speed and Energy

Impact speed, ft/sec	Impact energy, ft-lb
0	0
50	.25
100	1.02
150	2.29
200	4.07
250	6.35
300	9.15
350	12.4
400	16.3
450	20.6
500	25.4
550	30.7

Table III. Graphite-Epoxy Material Properties

Longitudinal Young's modulus, psi	18.5×10^6
Transverse Young's modulus, psi	1.64×10^6
Shear modulus, psi	8.9×10^5
Major Poisson's ratio	0.30

Table IV. Tension-Loaded Specimens

Nominal impact speed, ft/sec	Normalized failure load, P_f/A,* ksi, at—	
	$x/b^{\dagger} = 0.5$	$x/b^{\dagger} = 0.2$
Stacking sequence $[(\pm 45)_2/\overline{90}]_s$		
200	27.2	24.6
300	23.2	16.8
400	22.6	19.3
Stacking sequence $[\pm 45/0_2]_s$		
100	116	
200	103	105
300	98	91
400	105	116

*$A = 0.149$ in^2 for $[(\pm 45)_2/\overline{90}]_s$ specimens and 0.131 in^2 for $[\pm 45/0_2]_s$ specimens.

†$b = 3$ in.

Table V. Compression-Loaded 3-in-Wide Specimens

Nominal impact speed, ft/sec	Normalized failure load, P/A,* ksi, for—					
	Graphite-epoxy tape		Graphite-thermoplastic tape		Graphite-thermoplastic fabric	
	$x/b^{\dagger} = 0.5$	$x/b^{\dagger} = 0.25$	$x/b^{\dagger} = 0.5$	$x/b^{\dagger} = 0.25$	$x/b^{\dagger} = 0.5$	$x/b^{\dagger} = 0.25$
Stacking sequence $[(\pm 45)_2/\overline{90}]_s$						
100	20.2	20.5	21.6	21.9	22.9	23.8
175	20.7	15.6	21.5	18.4	23.7	22.0
225	17.8					
250	18.5	12.9	17.5	16.4	19.1	17.8
300	18.8		12.7			
325		15.6	13.6	12.3	17.8	14.8
350	17.8		16.2			
375					16.5	
400	19.2		16.3		18.1	13.6
400			13.9			
500			17.6			
Stacking sequence $[(\pm 45)_2/90]_{3s}$						
100	51.4	50.7				
175	27.0	29.0				
250	19.6	22.7				
325	16.0					
400	15.2	15.5				
540	20.2	17.0				

*$A = 0.144$, 0.147, and 0.141 in^2, for the graphite-epoxy, graphite-thermoplastic tape, and graphite-thermoplastic fabric $[(\pm 45)_2/\overline{90}]_s$ specimens, respectively. $A = 0.488$ in^2 for the $[(\pm 45)_2/90]_{3s}$ specimens.

$^{\dagger}b = 3$ in.

Table VI. Compression-Loaded 4-in-Wide Specimens

Material	Nominal impact speed, ft/sec	Normalized failure load, P/A,* ksi, at—		
		$x/b^{\dagger} = 0.5$	$x/b^{\dagger} = 0.3$	$x/b^{\dagger} = 0.2$
Stacking sequence $[(\pm 45)_2/\overline{90}]_s$				
Graphite-epoxy tape	450	15.9	17.0	8.7
Graphite-thermoplastic tape	450	18.2		9.5
Graphite-thermoplastic fabric	450	18.1	13.8	12.2
Stacking sequence $[(\pm 45)_2/90]_{3s}$				
Graphite-epoxy tape	500	21.0	18.3	15.5

*$A = 0.192$, 0.198, and 0.184 in^2, for the graphite-epoxy, graphite-thermoplastic tape, and graphite-thermoplastic fabric $[(\pm 45)_2/\overline{90}]_s$ specimens, respectively. $A = 0.644$ in^2 for the $[(\pm 45)_2/90]_{3s}$ specimens.
†$b = 4$ in.

Table VII. Compression-Loaded 10-in-Wide Specimens

Nominal impact speed, ft/sec	Normalized failure load, P/A,* ksi, at—		
	$x/b^{\dagger} = 0.5$	$x/b^{\dagger} = 0.2$	$x/b^{\dagger} = 0.1$
Stacking sequence $[\pm 45/0_2/]_{3s}$			
250	23.4	21.8	
350	21.0	21.6	16.2
450	20.9	21.2	14.3
Stacking sequence $[\pm 45/0_2/]_s$			
150	9.98		9.1

*$A = 0.428$ in^2 for $[\pm 45/0_2]_s$ specimens and 1.28 in^2 for $[\pm 45/0_2]_{3s}$ specimens.
†$b = 10$ in.

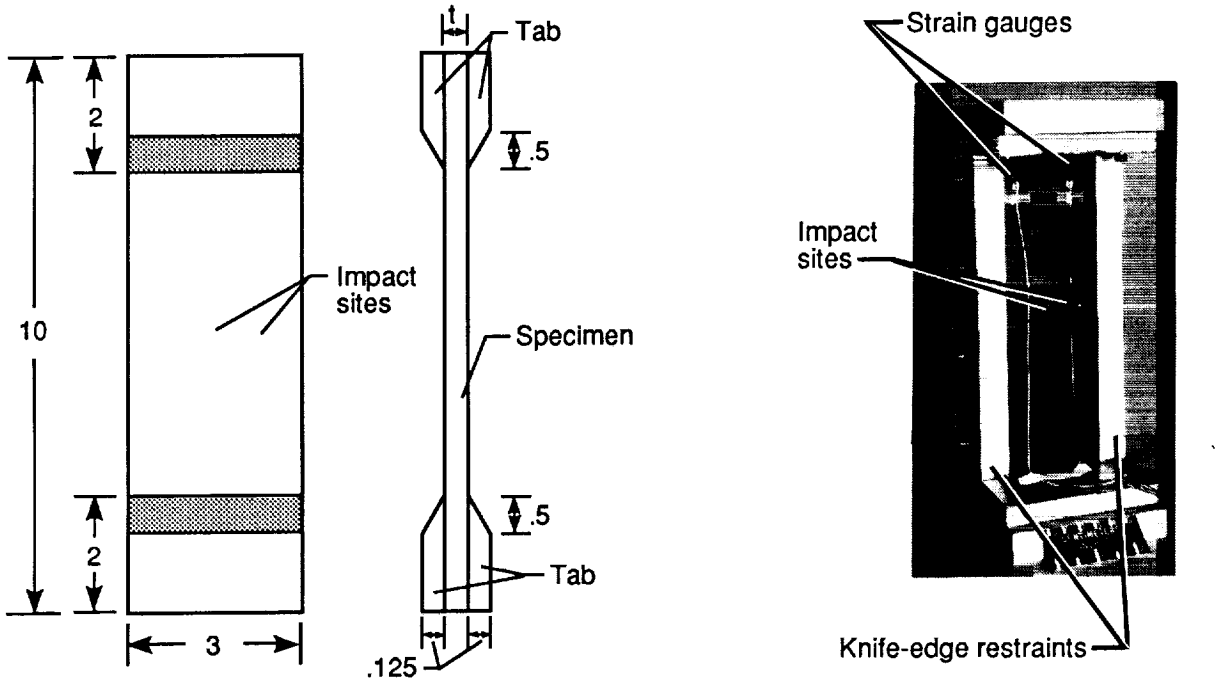

(a) Tension-loaded specimens.

(b) Compression-loaded specimens.

Figure 1. Specimen configuration. Dimensions are in inches.

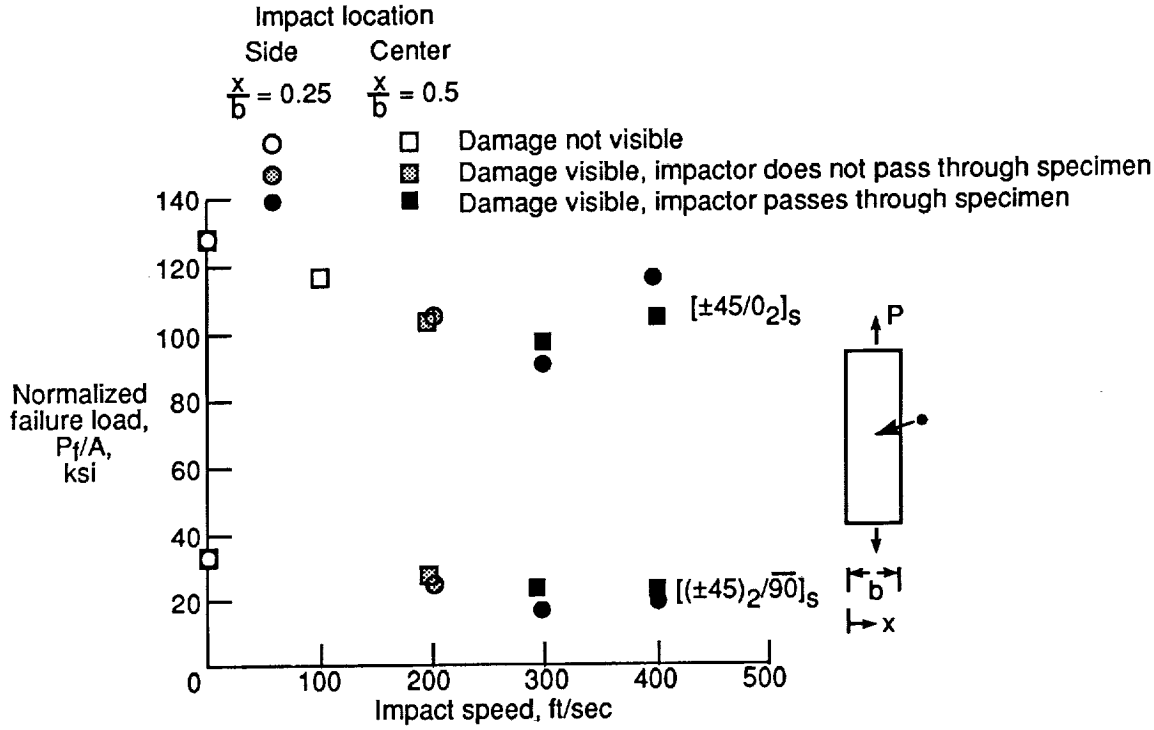

Figure 2. Effect of impact speed on normalized tensile failure load.

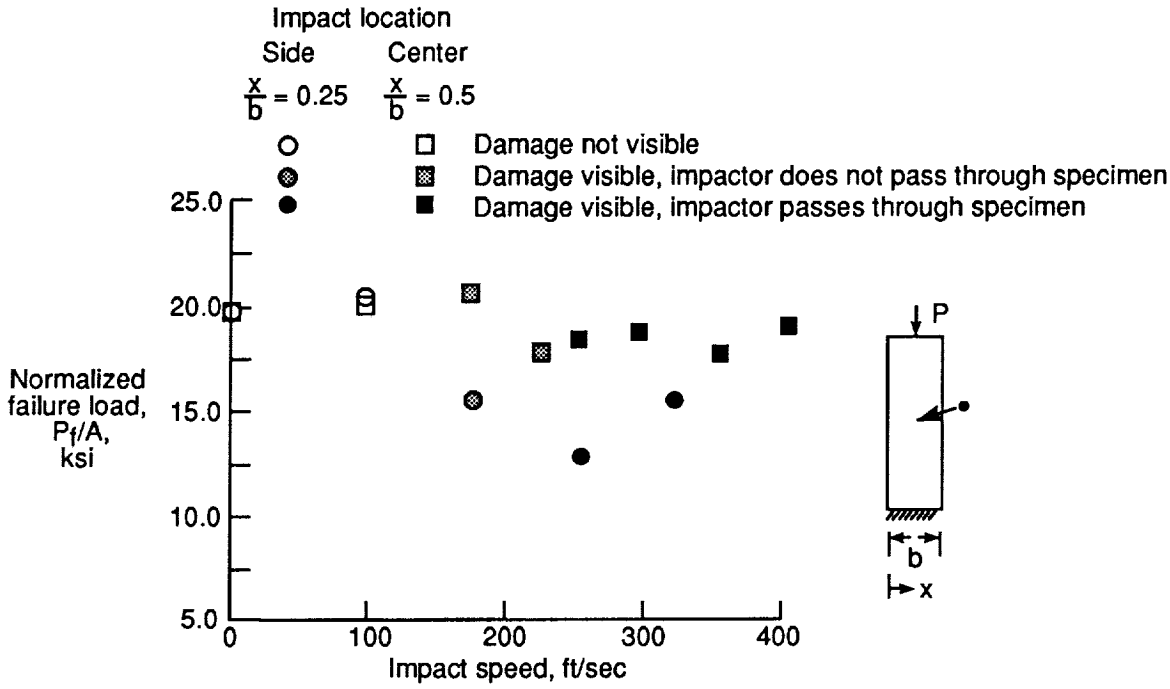

(a) Graphite-epoxy tape specimens.

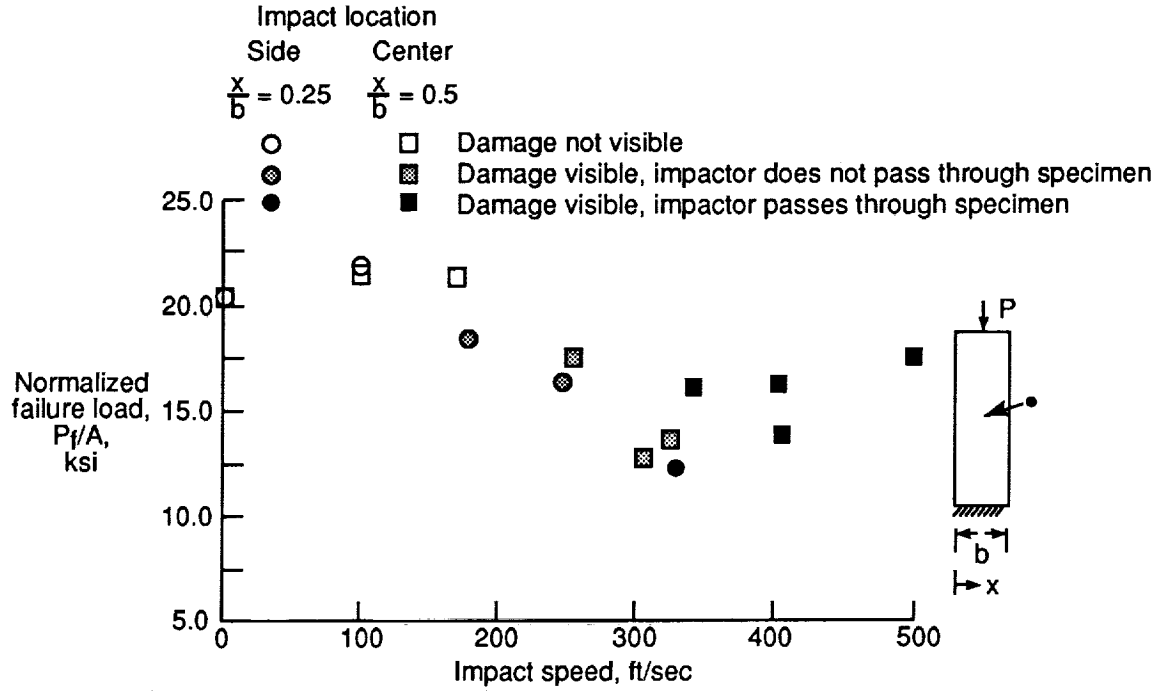

(b) Graphite-thermoplastic tape specimens.

Figure 3. Effect of impact speed on compressive failure load for panels with stacking sequence $[(\pm 45)_2/\overline{90}]_s$.

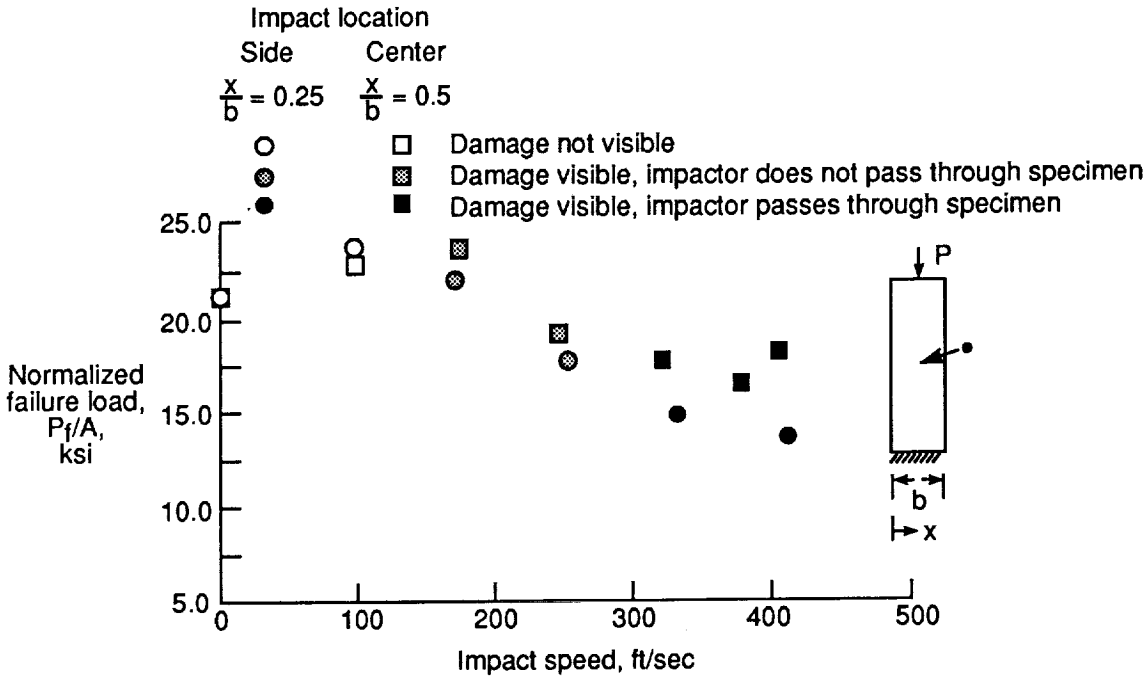

(c) Graphite-thermoplastic fabric specimens.

Figure 3. Concluded.

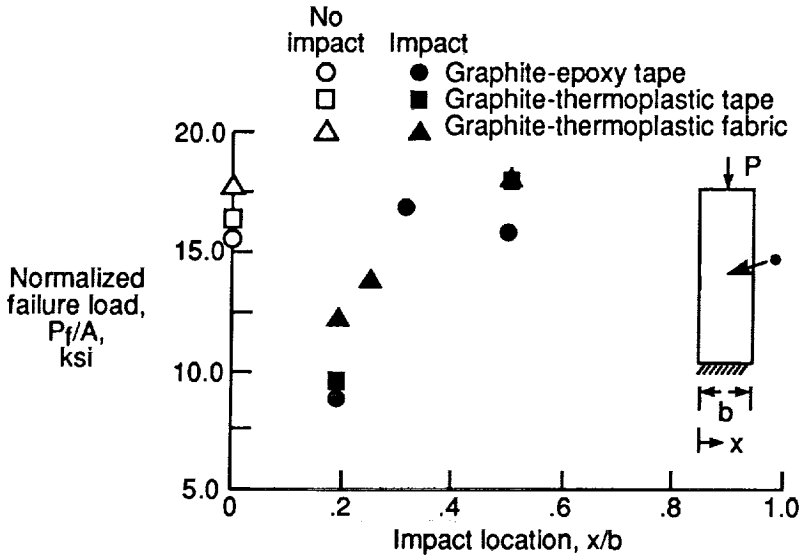

Figure 4. Normalized compressive failure load as function of impact location for panels with stacking sequence $[(\pm 45)_2/\overline{90}]_s$ impacted at 450 ft/sec.

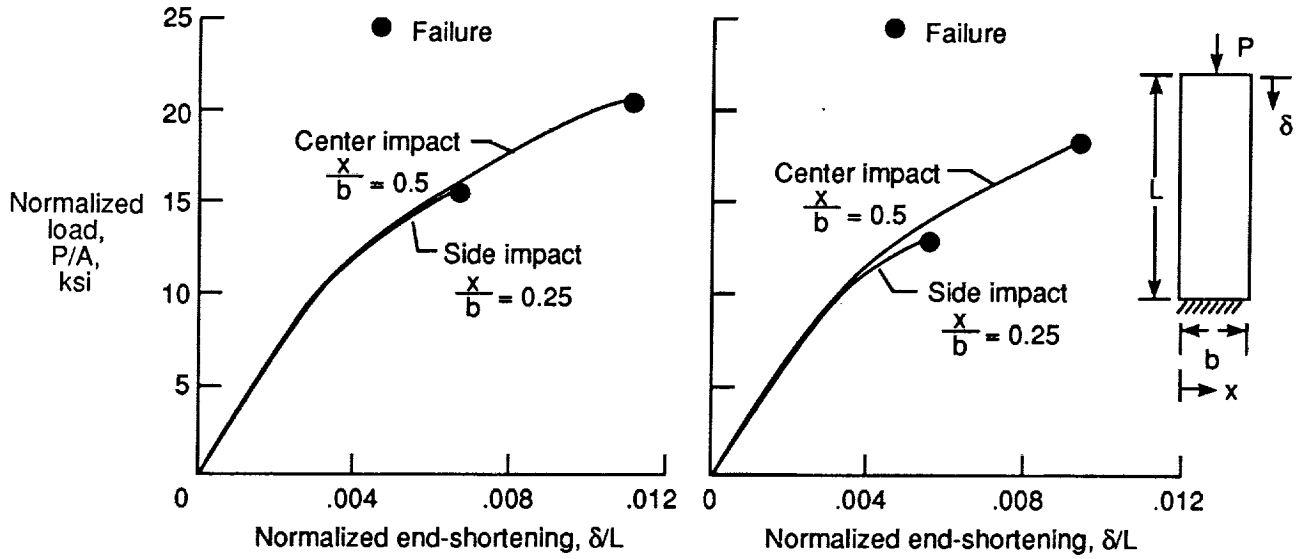

(a) Impact damage barely visible prior to load; impact speed, 175 ft/sec.

(b) Severe impact damage; impact speed, 250 ft/sec.

Figure 5. Normalized load versus normalized end-shortening for graphite-epoxy panels with stacking sequence $[(\pm 45)_2/\overline{90}]_s$.

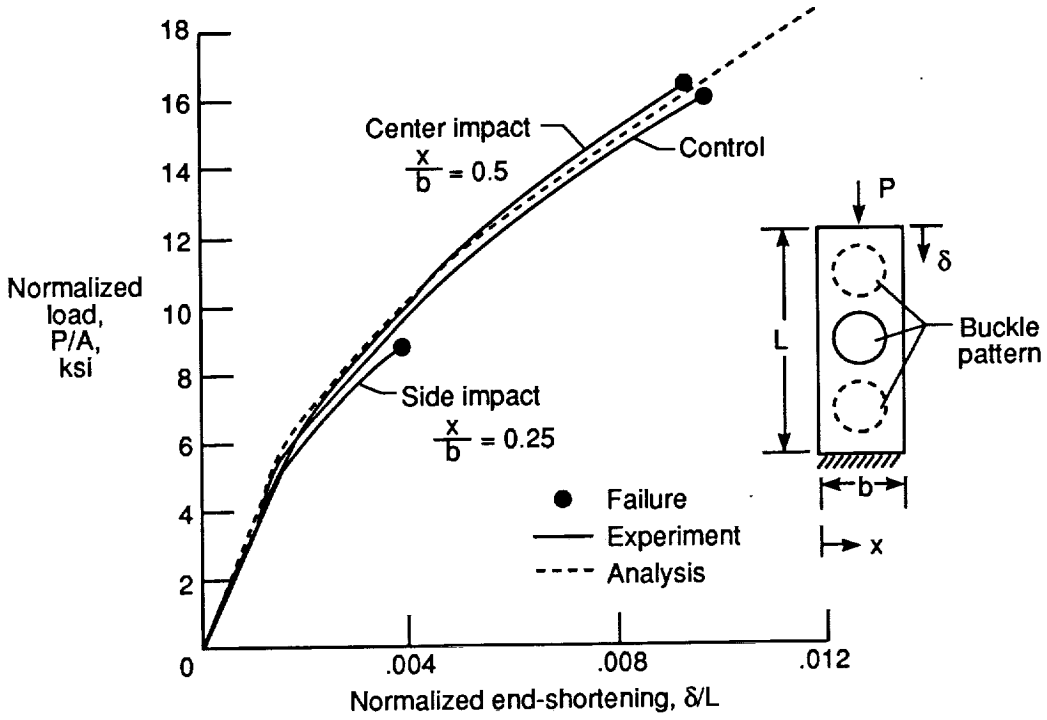

(a) Normalized load versus normalized end-shortening.

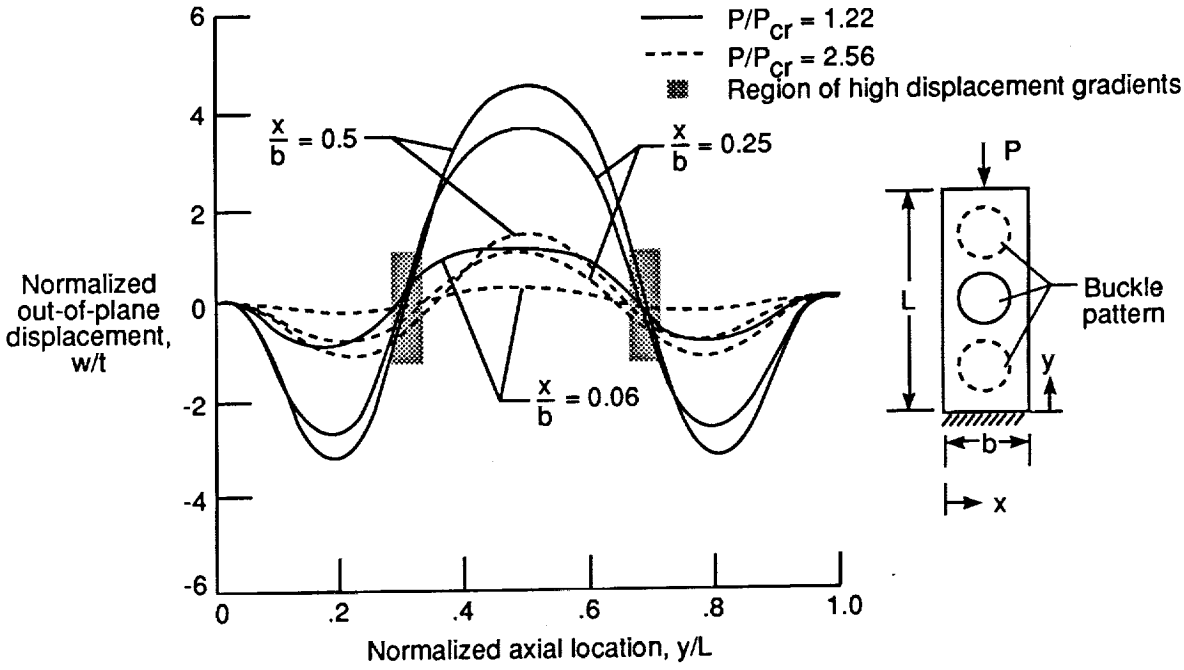

(b) Axially determined normalized out-of-plane displacement versus normalized axial location at two values of load.

Figure 6. Displacements and strains for 4-in-wide control panels with stacking sequence $[(\pm 45)_2/\overline{90}]_s$.

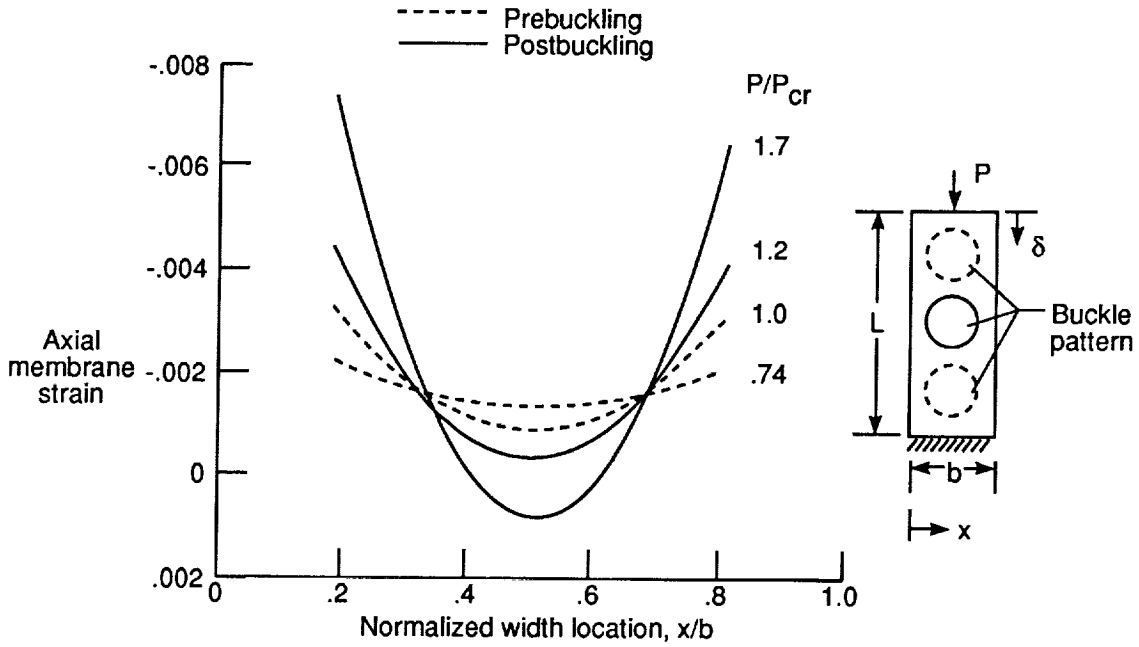

(c) Experimentally determined axial membrane strain versus normalized width location for various load levels at nodal line.

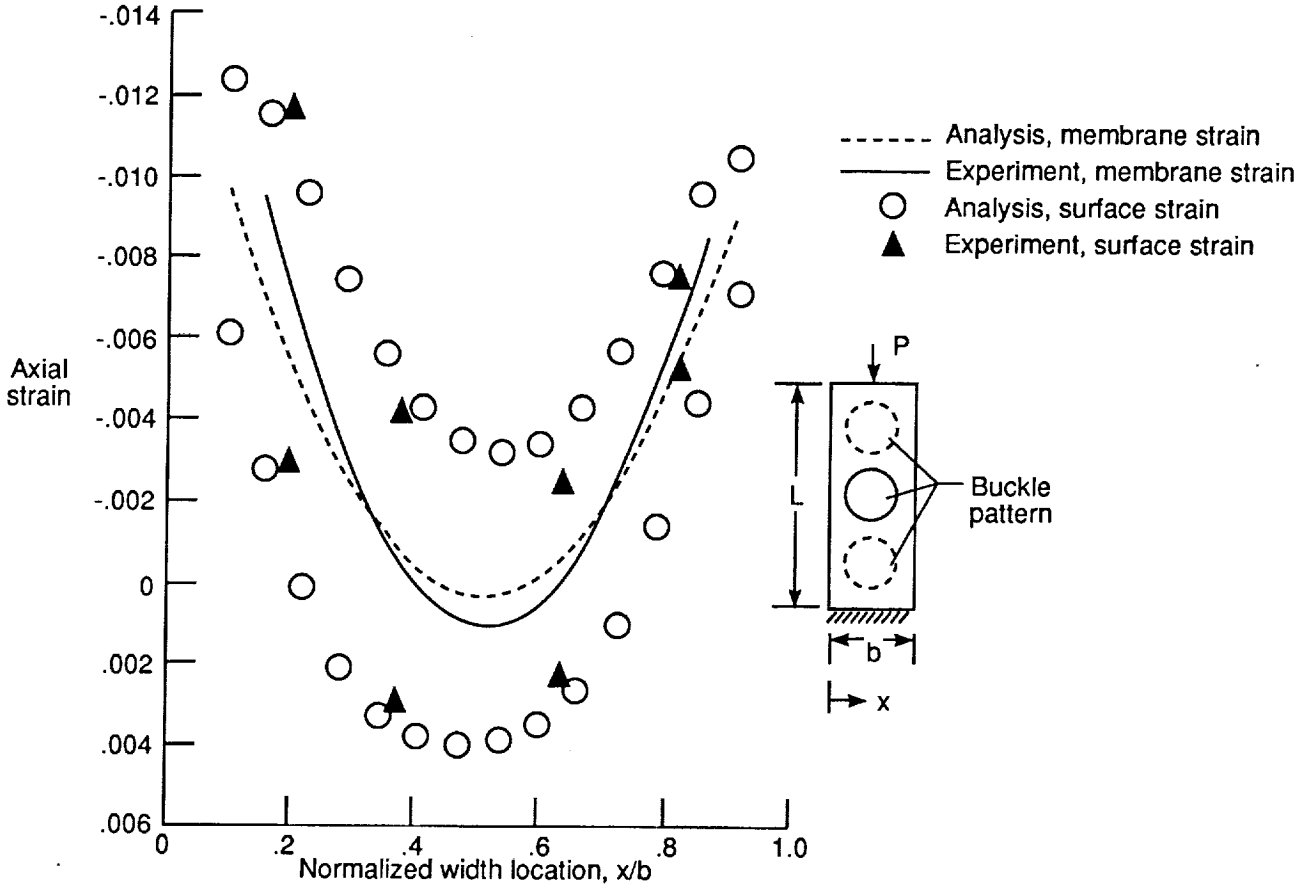

(d) Axial strain versus normalized width location at failure.

Figure 6. Concluded.

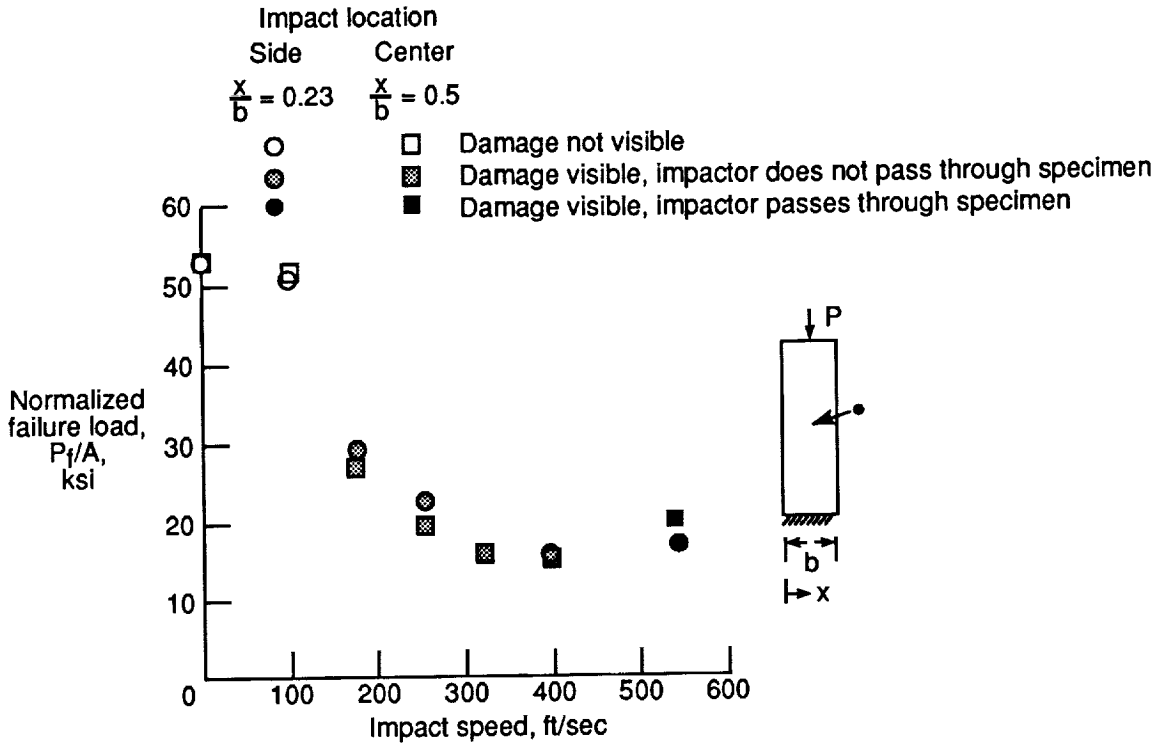

Figure 7. Effect of impact speed on normalized compressive failure load for panels with stacking sequence $[(\pm 45)_2/\overline{90}]_{3s}$.

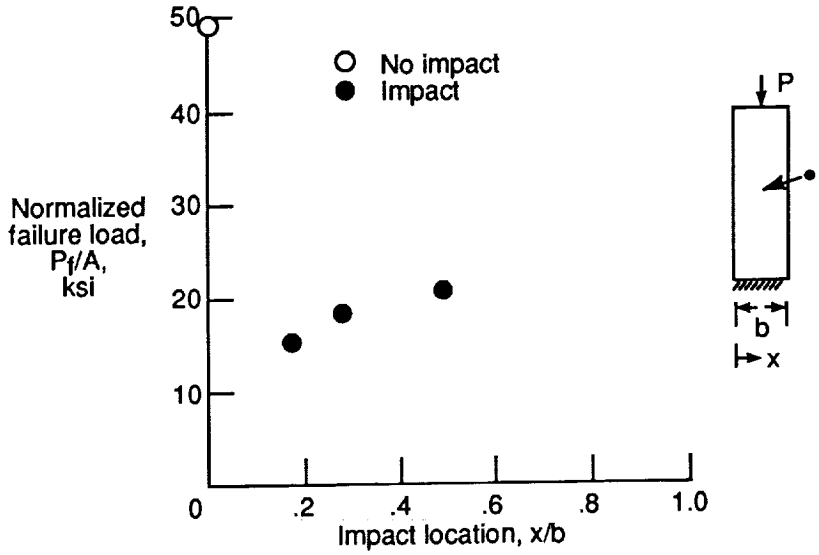

Figure 8. Normalized compressive failure load as function of impact location for 4-in-wide panels with stacking sequence $[(\pm 45)_2/90]_{3s}$ impacted at 500 ft/sec.

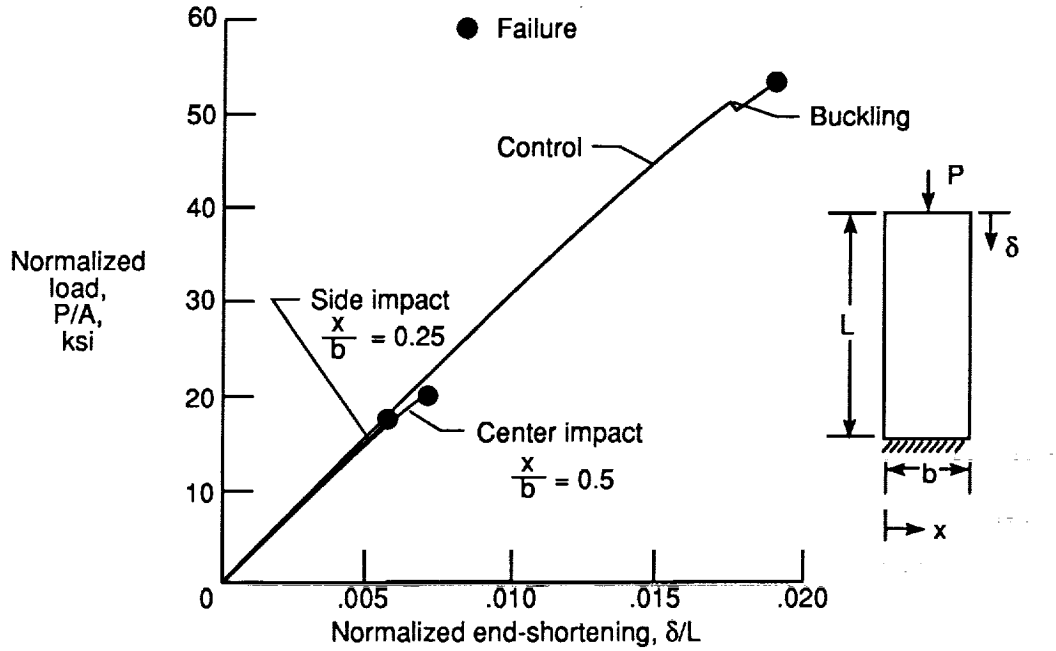

Figure 9. Normalized load versus normalized end-shortening for graphite-epoxy panels with stacking sequence $[(\pm 45)_2/90]_{3s}$ with no impact and with impact at center or side at 540 ft/sec.

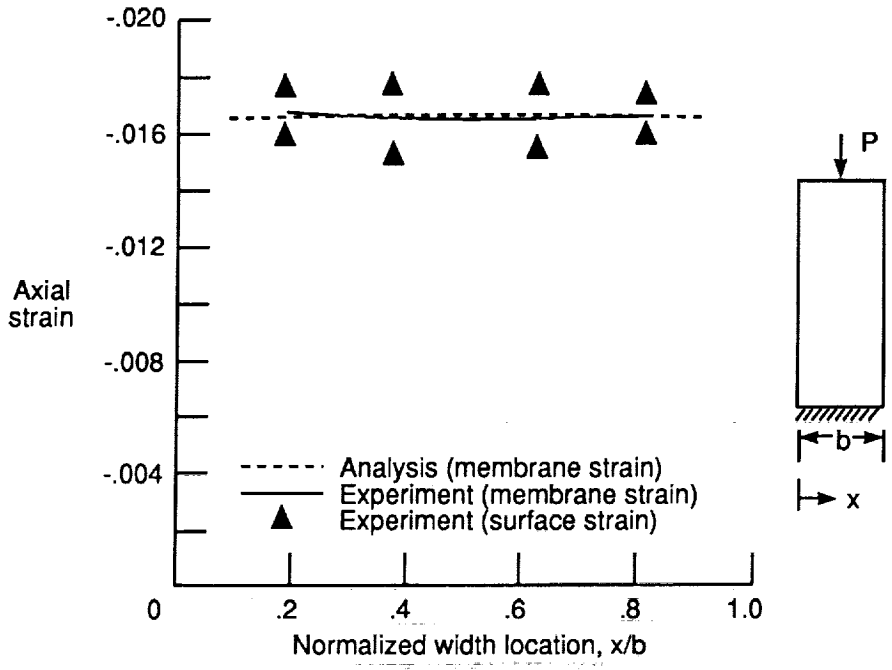

Figure 10. Axial strain versus normalized width location at failure of 4-in-wide control panel with stacking sequence $[(\pm 45)_2/90]_{3s}$.

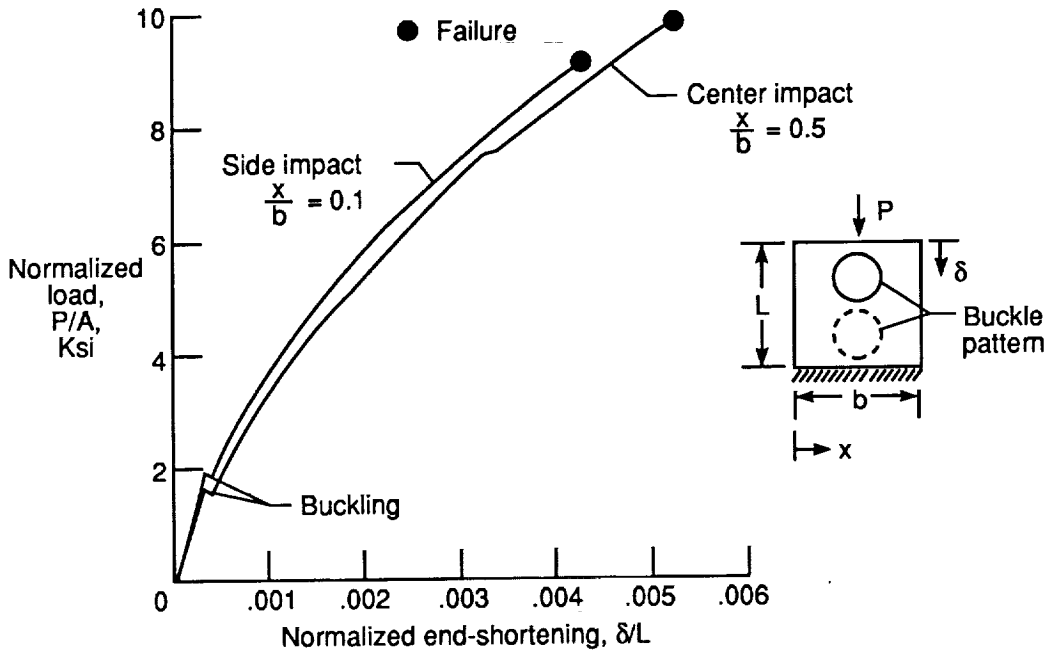

Figure 11. Normalized load versus normalized end-shortening for graphite-epoxy panels with stacking sequence $[(\pm 45/0_2]_s$ impacted at center or side with impact speed of 150 ft/sec. Impact caused barely visible damage prior to load.

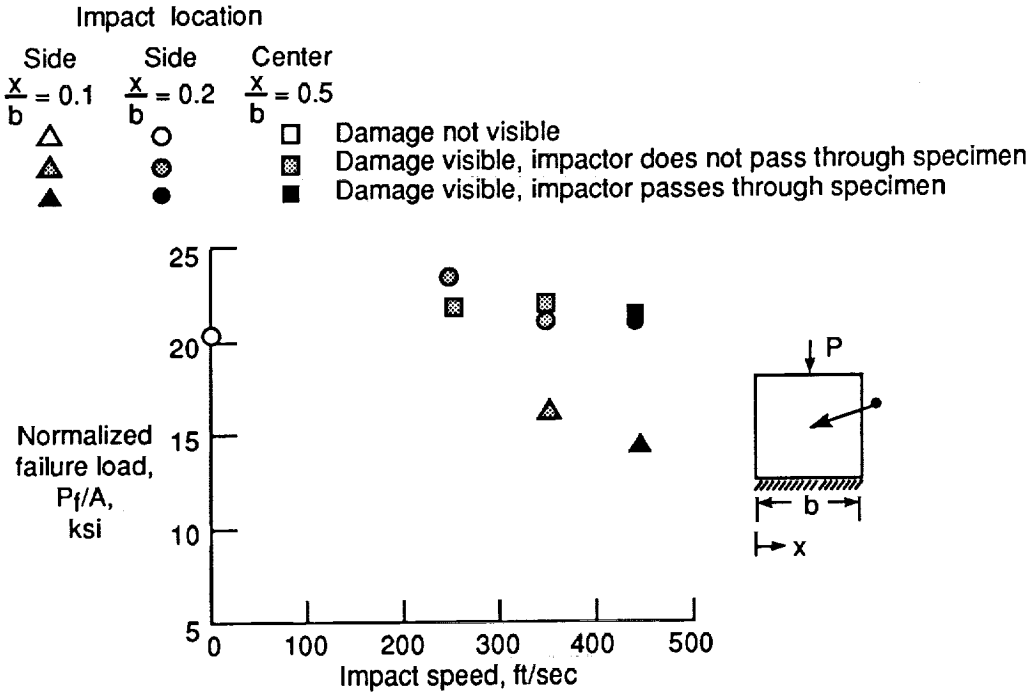

Figure 12. Effect of impact speed on normalized compressive failure load of graphite-epoxy panels with stacking sequence $[\pm 45/0_2]_{3s}$.

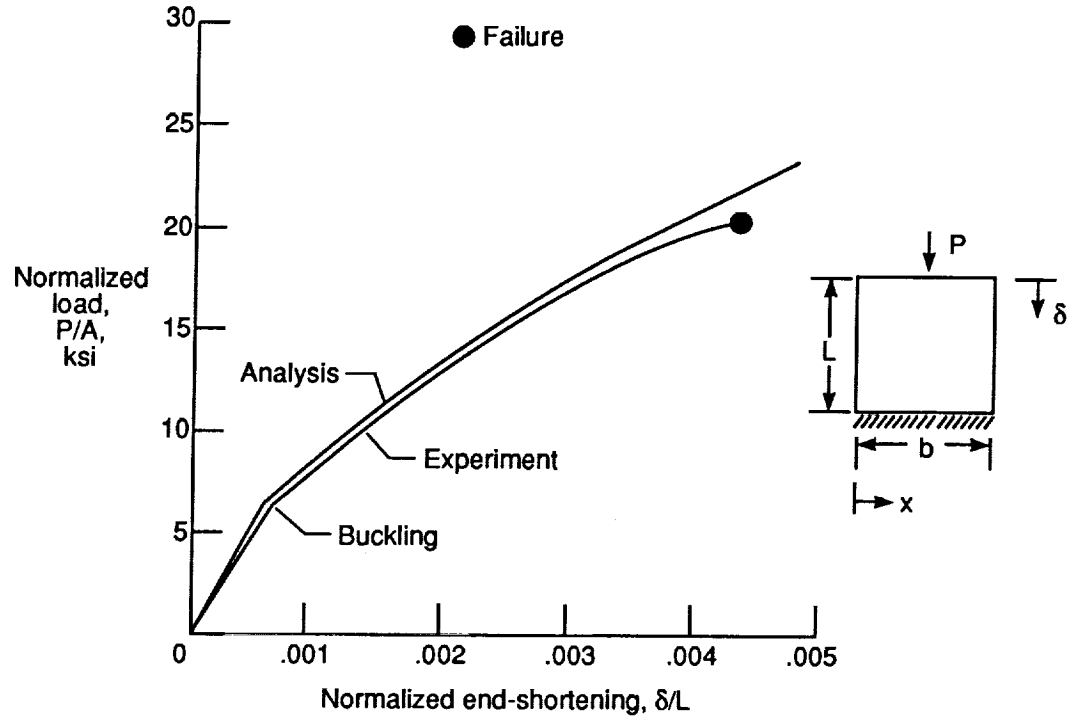

Figure 13. Normalized load versus normalized end-shortening for control panel with stacking sequence $[\pm 45/0_2]_{3s}$.

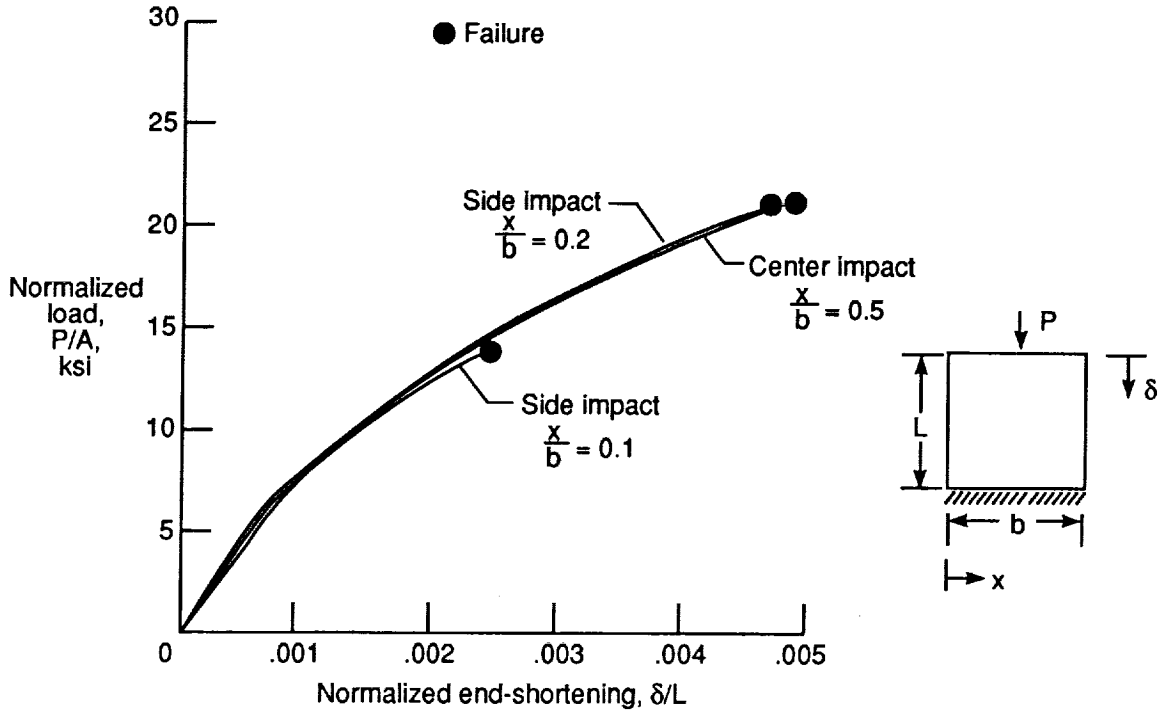

Figure 14. Normalized load versus normalized end-shortening for panels with stacking sequence $[\pm 45/0_2]_{3s}$ impacted at 450 ft/sec in center and at two side locations.

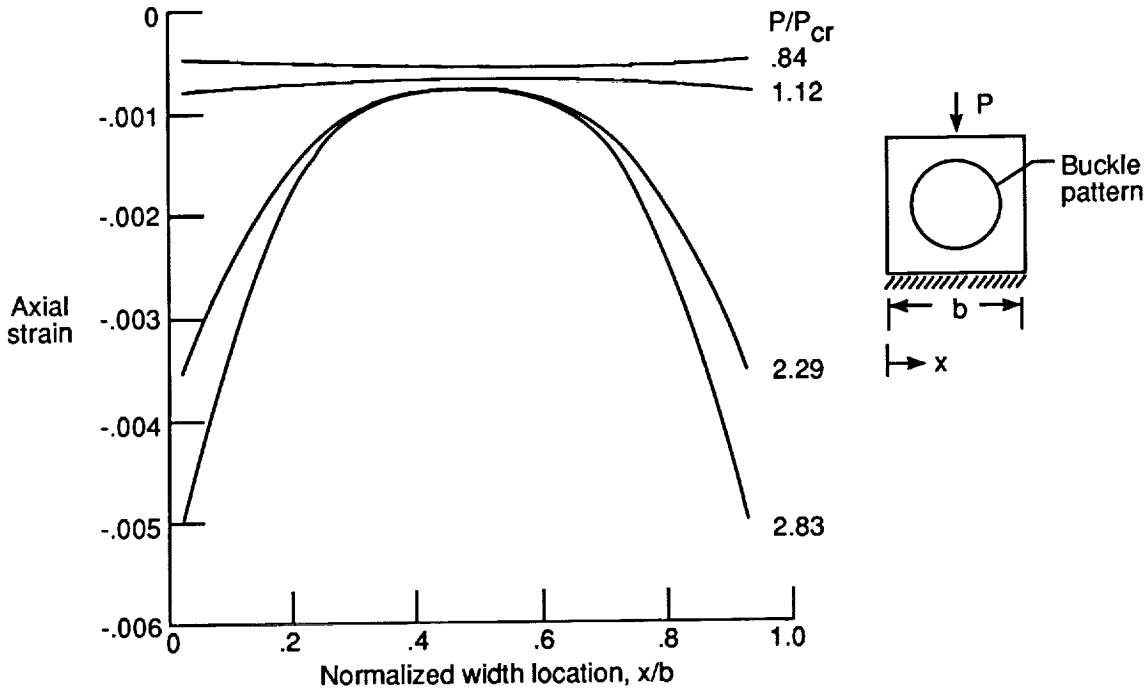

(a) Axial strain for several load levels.

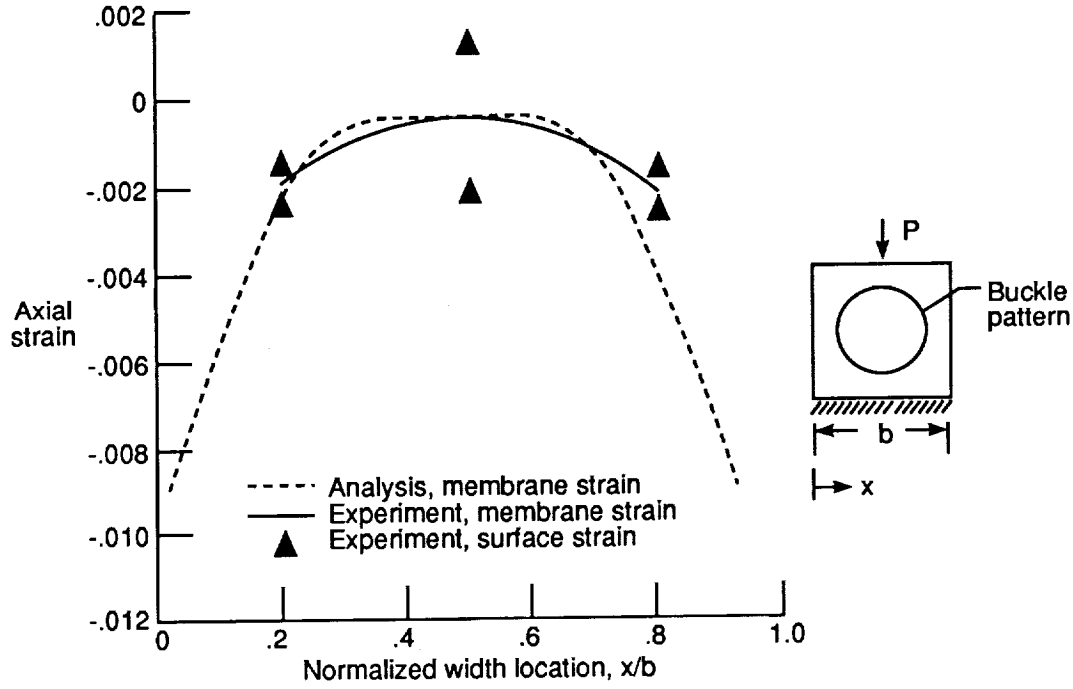

(b) Strain at failure.

Figure 15. Strain versus normalized width location of 10-in-wide control panel at axial centerline with stacking sequence $[\pm 45/0_2]_{3s}$.

REPORT DOCUMENTATION PAGE

Form Approved
OMB No. 0704-0188

1. AGENCY USE ONLY *(Leave blank)*	2. REPORT DATE	3. REPORT TYPE AND DATES COVERED
	May 1992	Technical Paper

4. TITLE AND SUBTITLE
Effect of Low-Speed Impact Damage and Damage Location on Behavior of Composite Panels

5. FUNDING NUMBERS
WU 505-63-50-08

6. AUTHOR(S)
Dawn C. Jegley

7. PERFORMING ORGANIZATION NAME(S) AND ADDRESS(ES)
NASA Langley Research Center
Hampton, VA 23665-5225

8. PERFORMING ORGANIZATION REPORT NUMBER
L-17031

9. SPONSORING/MONITORING AGENCY NAME(S) AND ADDRESS(ES)
National Aeronautics and Space Administration
Washington, DC 20546-0001

10. SPONSORING/MONITORING AGENCY REPORT NUMBER
NASA TP-3196

11. SUPPLEMENTARY NOTES
Presented at the 9th DoD/NASA/FAA Conference on Fibrous Composites in Structural Design, Lake Tahoe, NV, November 4 7, 1991.

12a. DISTRIBUTION/AVAILABILITY STATEMENT
Unclassified -Unlimited

Subject Category 24

12b. DISTRIBUTION CODE

13. ABSTRACT *(Maximum 200 words)*

The effect of low-speed impact damage on the compression and tension strength of thin and moderately thick composite specimens was investigated. Impact speeds ranged from 50 to 550 ft/sec, with corresponding impact energies from 0.25 to 30.7 ft-lb. Impact locations were at the center of the specimen or near a lateral unloaded edge. In this study, thin specimens with only 90° and ±45° plies that were impacted away from the unloaded edge suffered less reduction in maximum load-carrying capability because of impact damage than the same specimens impacted near the unloaded edge. Failure loads of thicker compression-loaded specimens with a similar stacking sequence were independent of impact location. Failure loads of thin tension-loaded specimens with 0° plies were independent of impact location, whereas failure loads of thicker compression-loaded specimens with 0° plies were dependent upon impact location. A finite-element analysis indicated that high axial strains occurred near the unloaded edges of postbuckled panels. Thus, impacts near the unloaded edge would significantly affect the behavior of the postbuckled panel.

14. SUBJECT TERMS	15. NUMBER OF PAGES
Impact damage; Graphite-epoxy; Postbuckling	26
	16. PRICE CODE A03

17. SECURITY CLASSIFICATION OF REPORT	18. SECURITY CLASSIFICATION OF THIS PAGE	19. SECURITY CLASSIFICATION OF ABSTRACT	20. LIMITATION OF ABSTRACT
Unclassified	Unclassified		

NSN 7540-01-280-5500

Standard Form 298(Rev. 2-89)
Prescribed by ANSI Std. Z39-18
298-102

NASA-Langley, 1992